



Meshing and Pore-Scale Simulation of Additively Manufactured Wicks in OpenFOAM

Marcus Ang^{*1}, Gisuk Hwang¹, Ikram Ahmed¹, Scott Roberts²

¹*Department of Mechanical Engineering, Wichita State University*

²*Jet Propulsion Laboratory, California Institute of Technology*

4/7/2023

Background: Why wicks?

- Wick structures are essential to design high heat flux two-phase thermal management systems.
- Wick structure facilitates greater heat transfer by passively transporting coolant via capillary action and prevent dry-out.

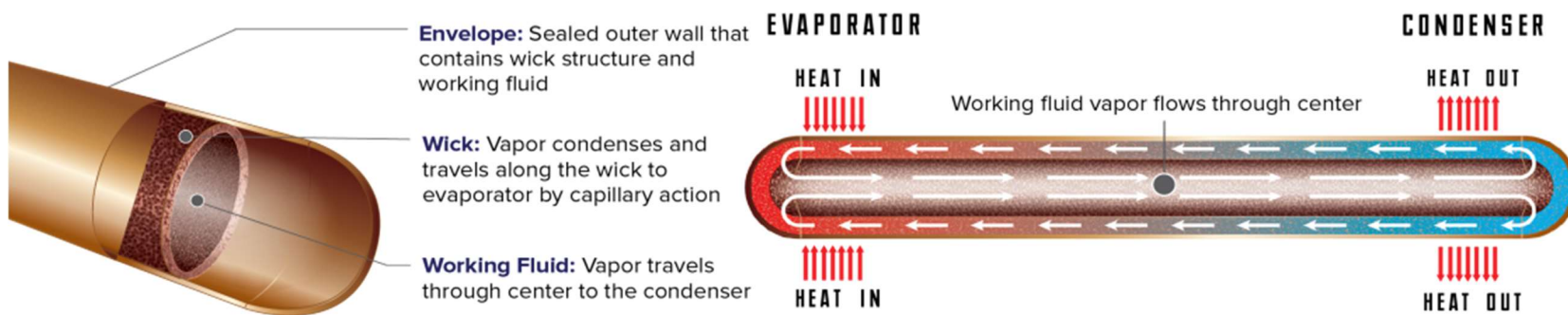


Fig. 1. Heat pipe porous wick structure and working principle. [1]

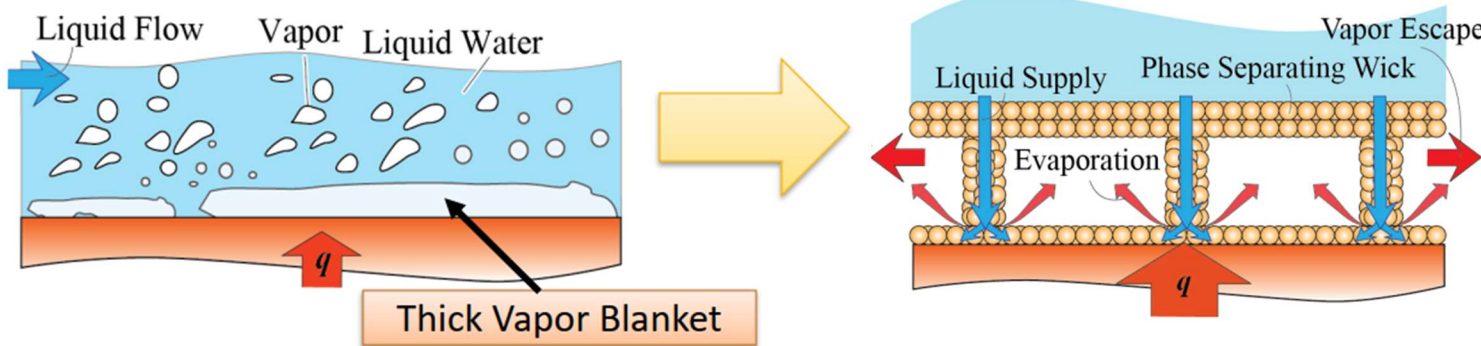


Fig. 2. Porous wicks to enhance critical heat flux (CHF) in pool boiling. [2]

Background: Why wicks?

- Depending on the application, the structure may be complex and highly non-uniform to obtain a desired heat and mass transfer properties.

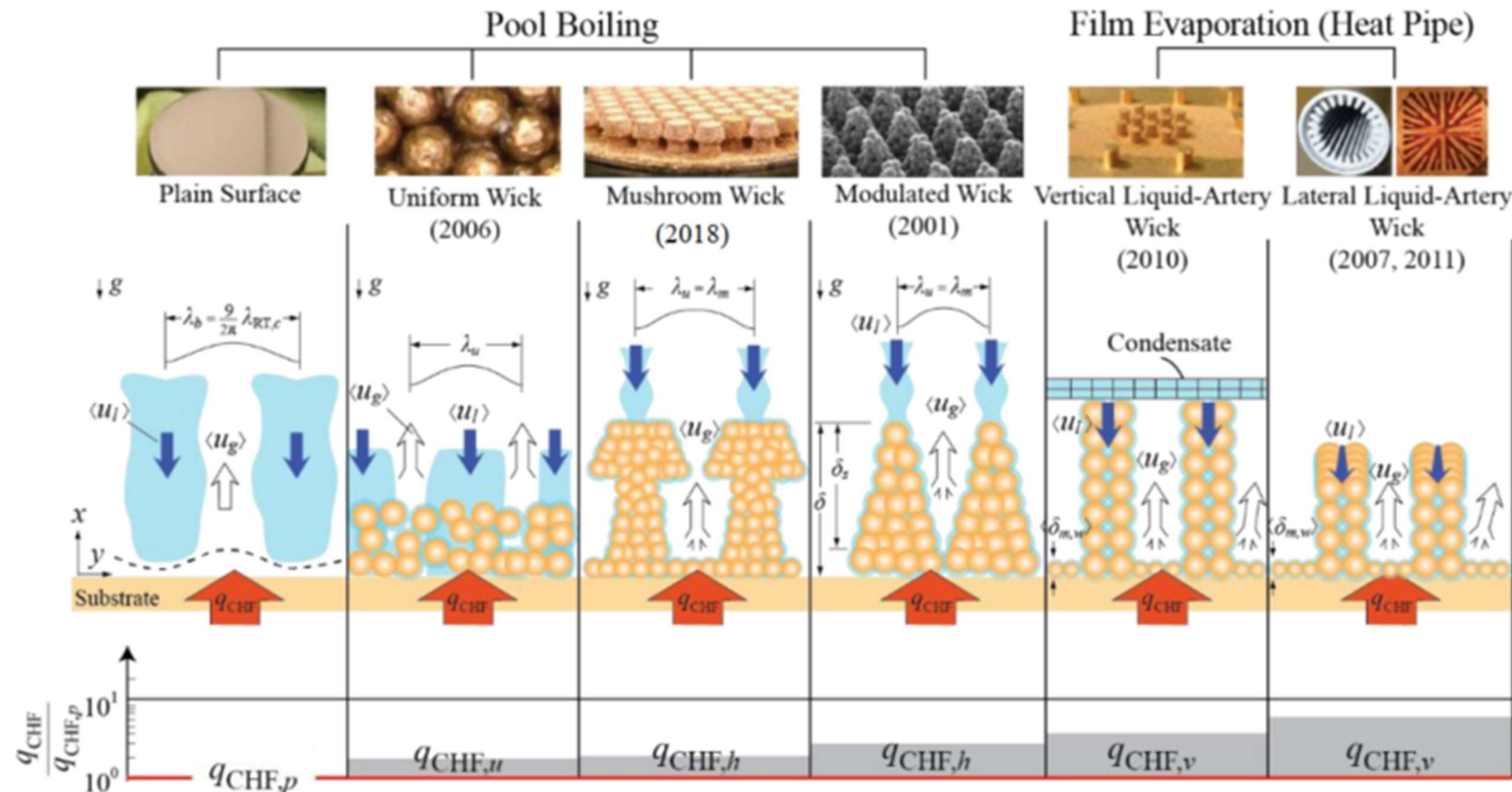


Fig. 3. Enhancement of critical heat flux (CHF) using porous wicks in pool boiling and film evaporation. [2]

Background: Manufacturing

- Laser Powder Bed Fusion (LPBF) additive manufacturing (AM) can precisely fabricate complex wick structure layer-by-layer.

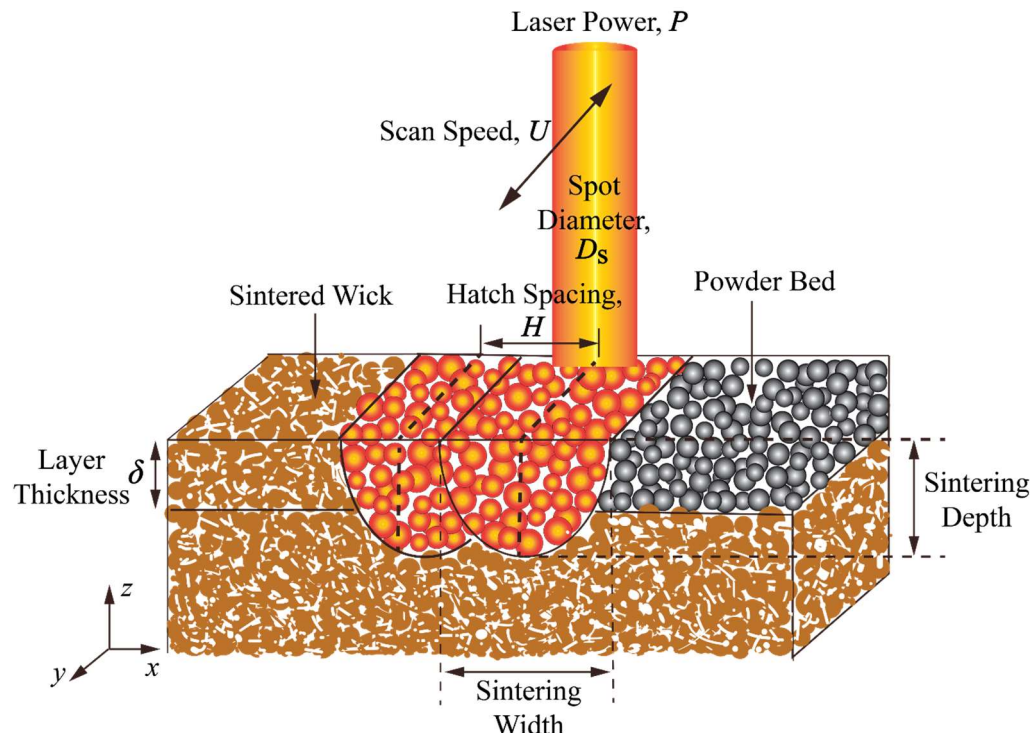


Fig. 4. Schematic of LPBF metal AM showing the main printing process parameters. [3]

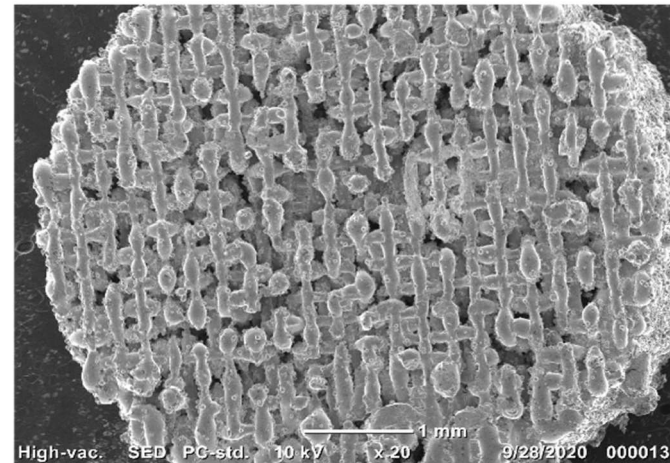


Fig. 5. Scanning electron microscope (SEM) image of AM wick [3]

Background: Modelling

- Empirical correlations cannot accurately predict key characteristic for non-uniform pore structures.
- Experimental characterizations are challenging and expensive.
- Micro-X-ray computed tomography (μ CT) can capture high resolution geometries of porous media for mesh generation to be used for computational fluid dynamics (CFD).

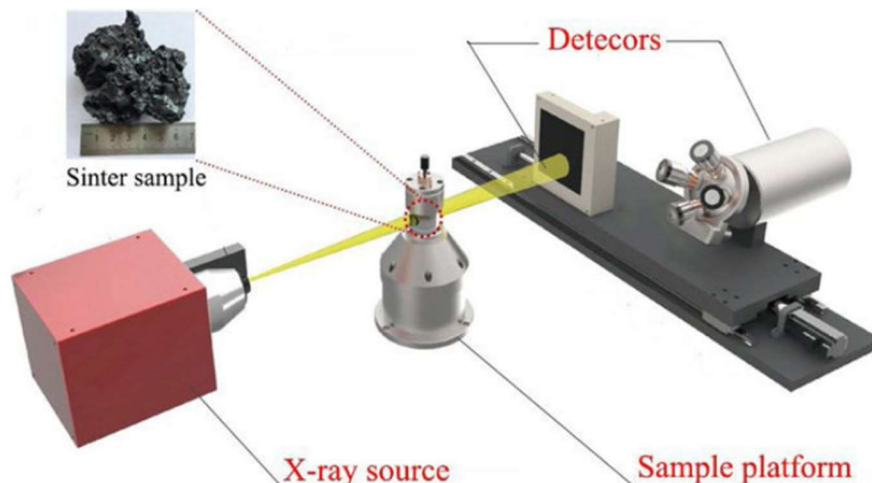


Fig. 6. Xray computed tomography system for sinter sample [4].

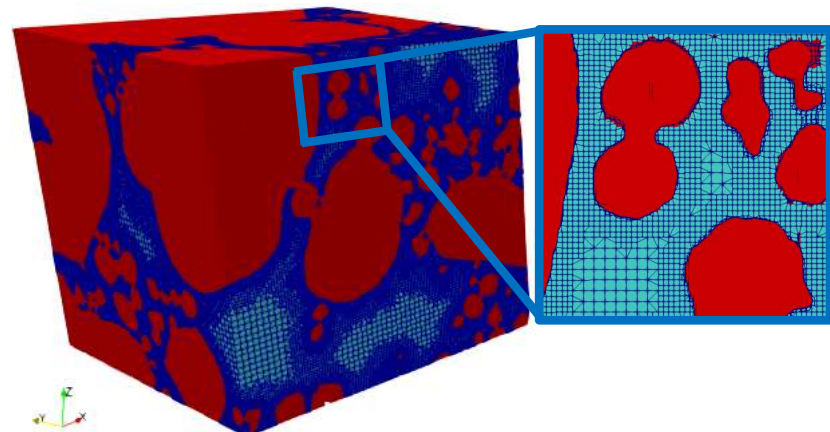


Fig. 7. $400 \times 400 \times 400 \mu\text{m}^3$ mesh for the fluid (blue) and solid (red) regions. Porosity is the ratio between pore volume and total volume.

Overview of Workflow

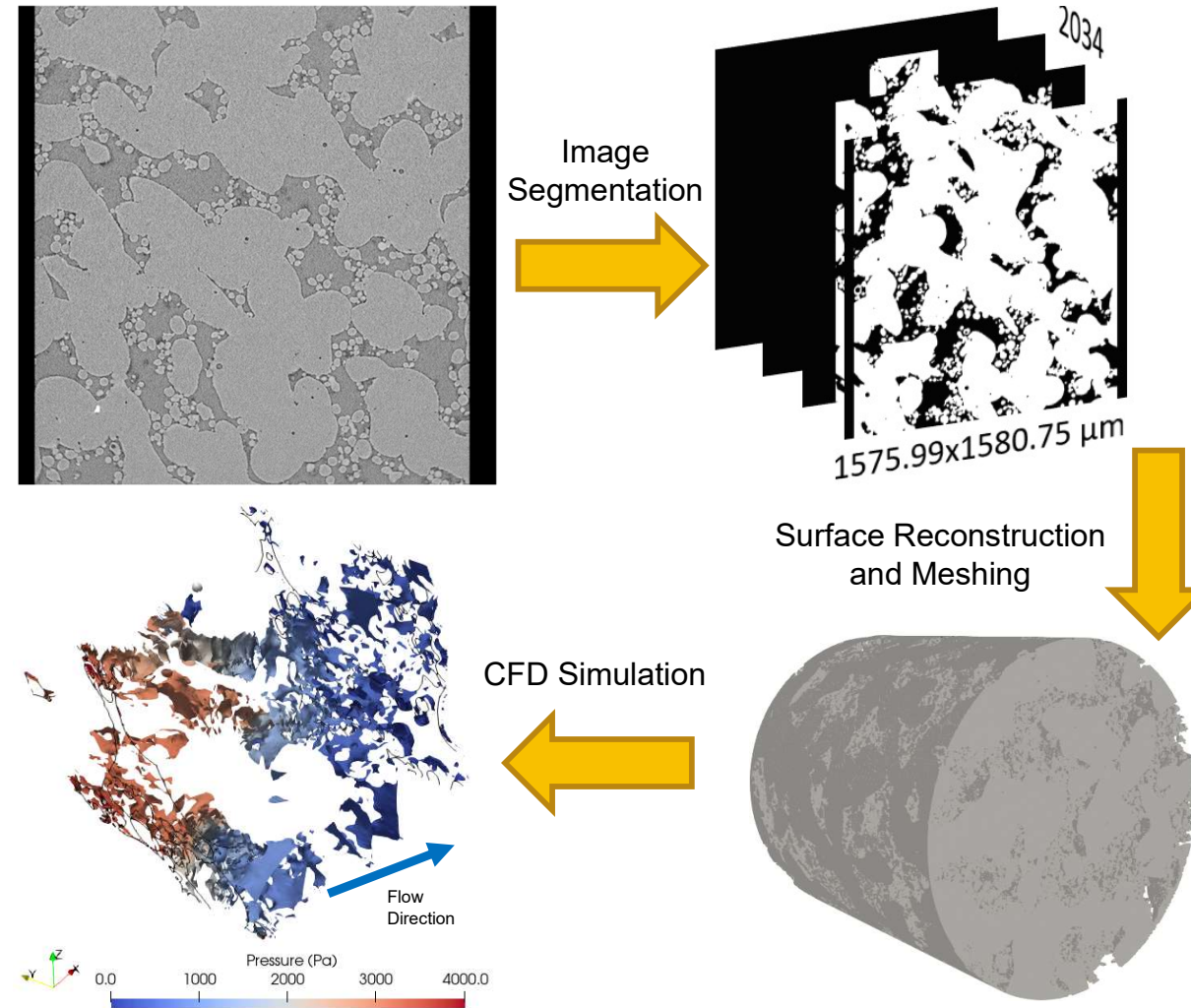


Fig. 8. Diagram of μ CT to CFD workflow.

Image Segmentation: Overview

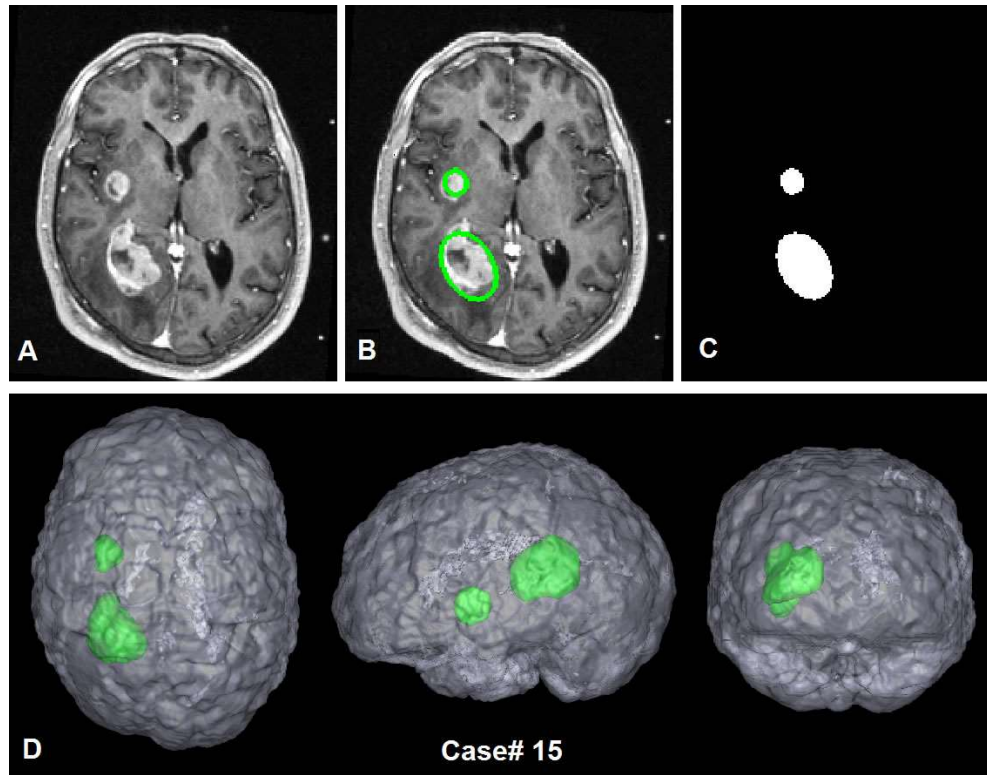


Fig. 9. 2-tumor-brain automatic detection and segmentation result [5]

- Goal is to separate an image or 3D model into regions of interest.
- Manual segmentation is challenging and time-consuming.
- Ideally, we want an automatic segmentation process.

Image Segmentation: Overview

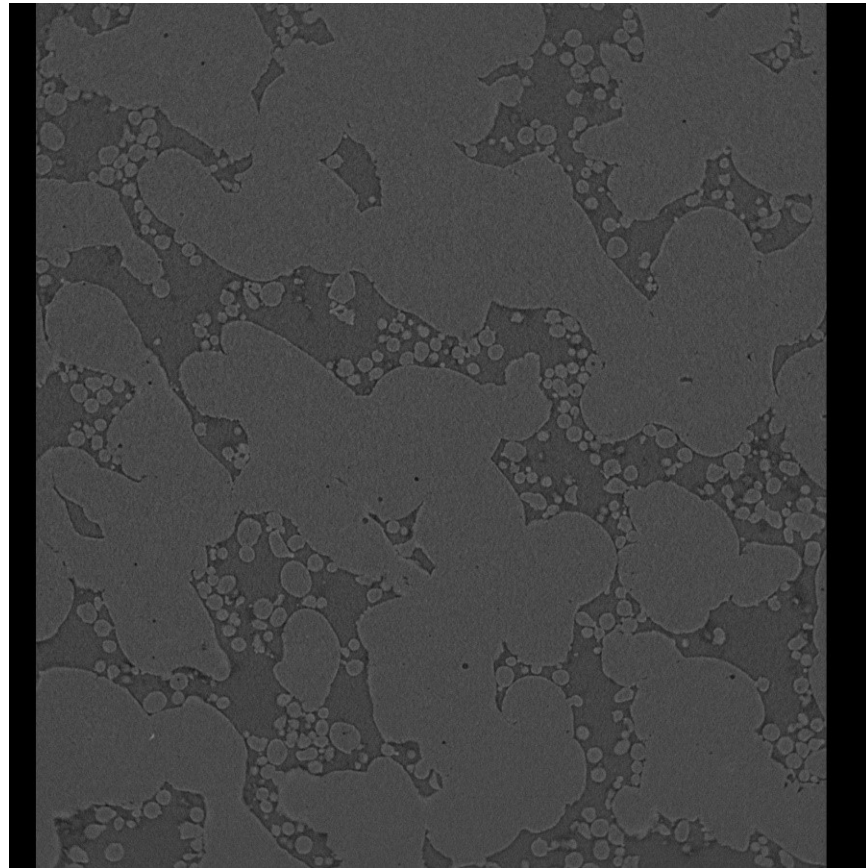


Fig. 10. μCT image 1333.

- Successful image segmentation requires filtering and thresholding.
- A filter must adequately reduce noise while preserving the edges.
- A threshold method must be robust to background noise and prevent pore collapse.

Image Segmentation: Overview

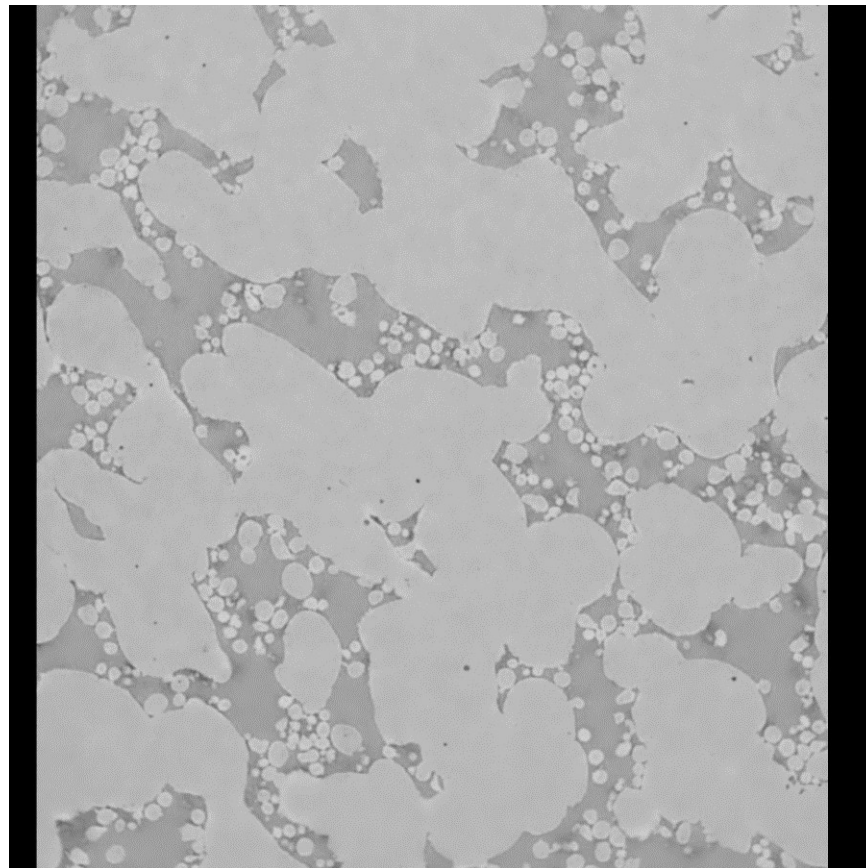


Fig. 11. Filtered image 1333.

- Successful image segmentation requires filtering and thresholding.
- A filter must adequately reduce noise while preserving the edges.
- A threshold method must be robust to background noise and prevent pore collapse.

Image Segmentation: Overview

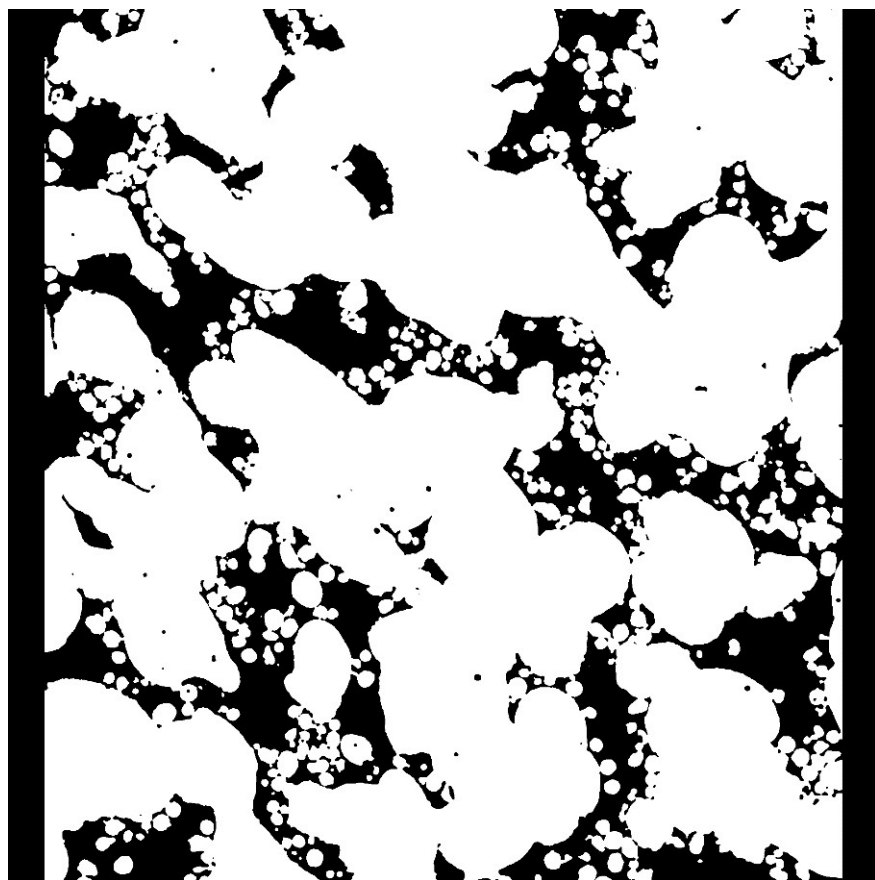


Fig. 12. Thresholded Image 1333 using Otsu's method.

- Successful image segmentation requires filtering and thresholding.
- A filter must adequately reduce noise while preserving the edges.
- A threshold method must be robust to background noise and prevent pore collapse.

Image Segmentation: Bilateral Filter

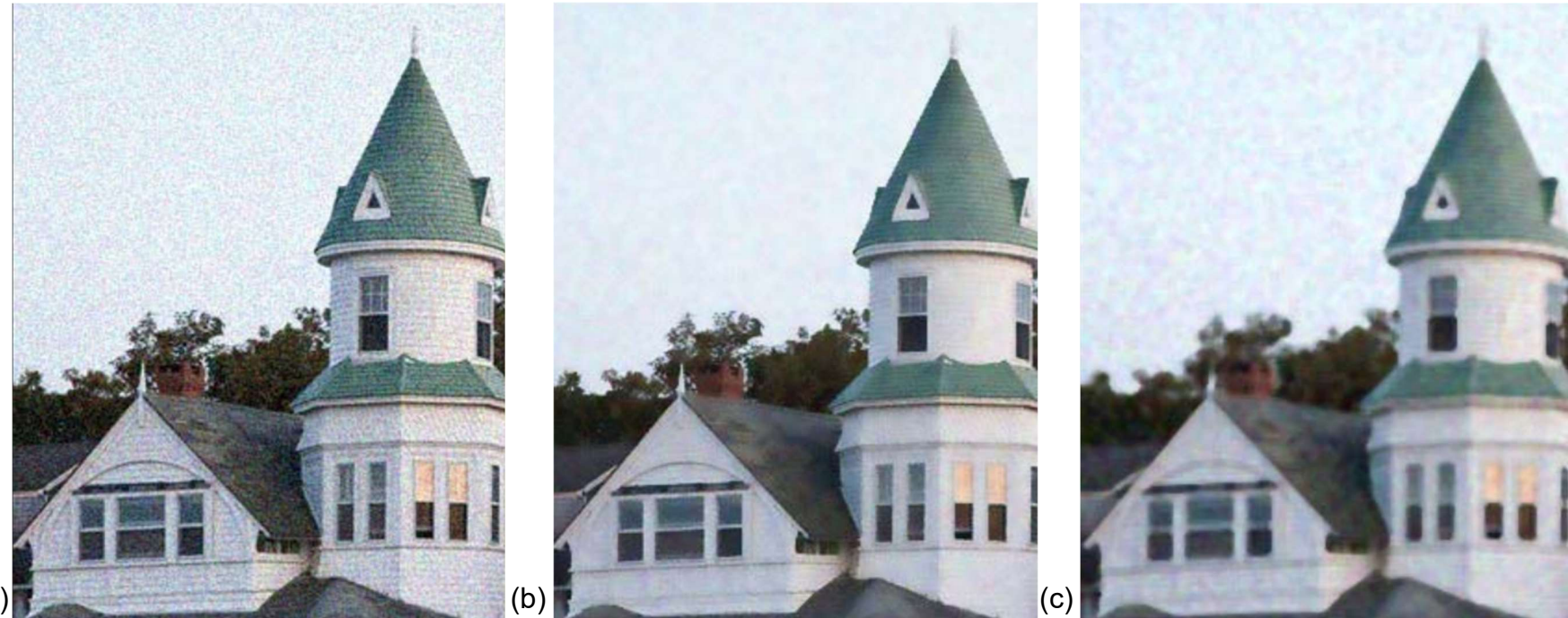


Fig. 13. Results of filtering using (a) no filter (b) bilateral filter and (c) median filter [6]

Image Segmentation: Filtering

- Bilateral filter requires 2 parameters, spatial and range.
- Parameter sensitivity study was performed on several images and 100 images that was cropped to $400 \times 400 \mu\text{m}^2$.

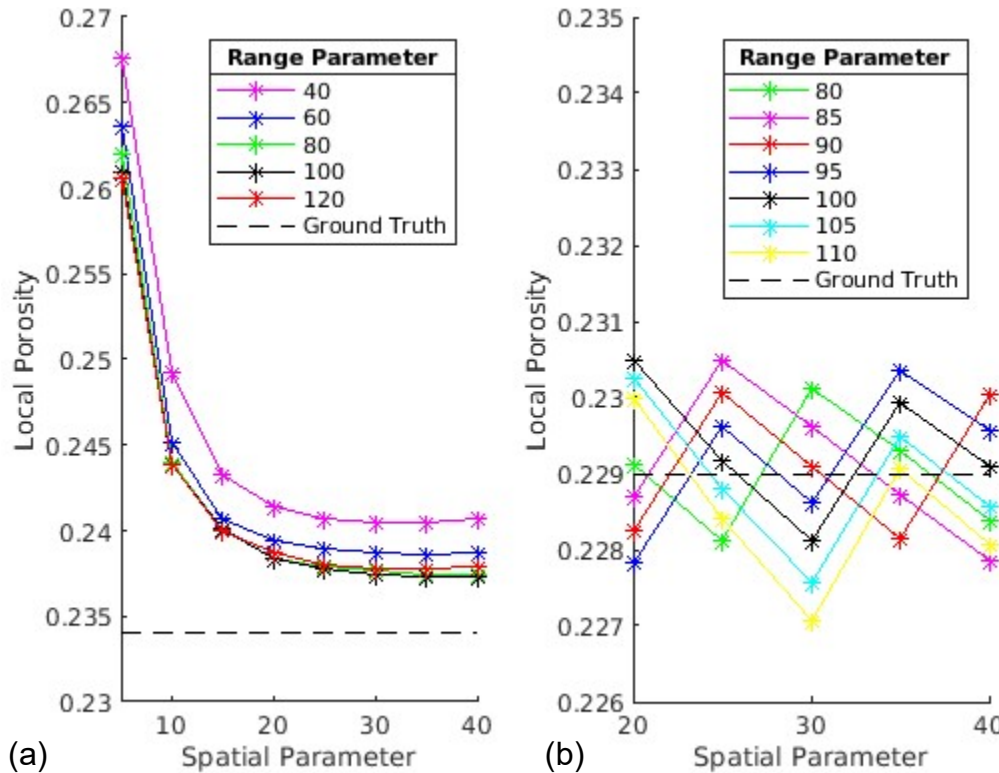


Fig. 14. Bilateral filter parameter sensitivity study on image (a) 1333 and (b) 200.

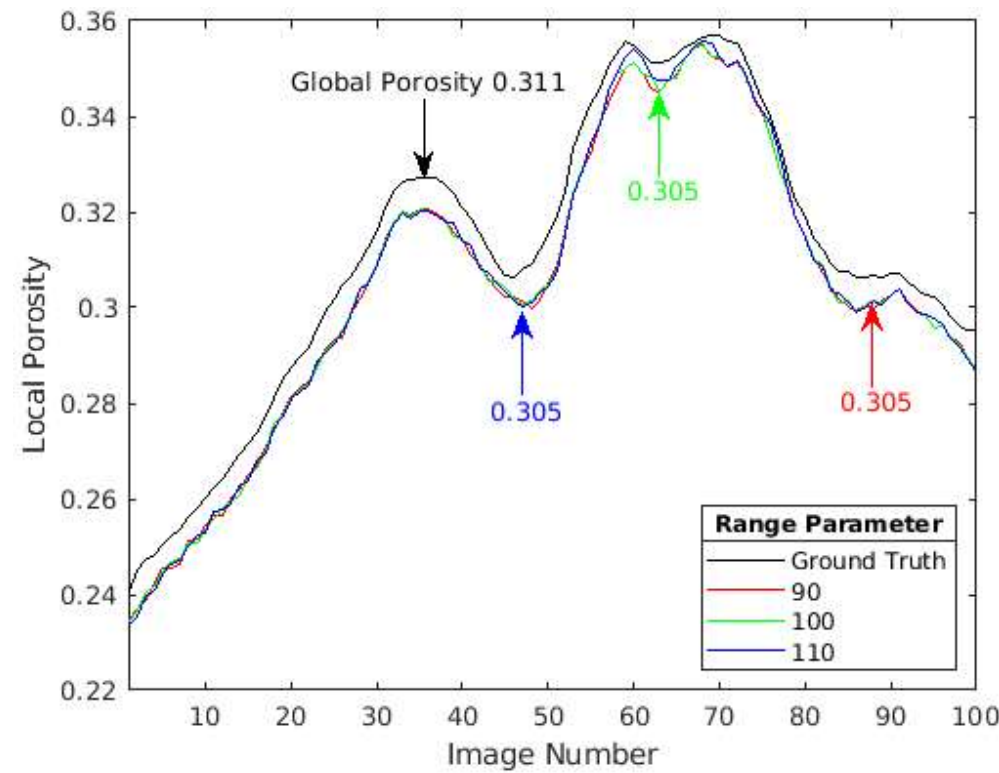


Fig. 15. Local and Global Porosity of $400 \times 400 \mu\text{m}^2$ image stack using selected parameter.

Image Segmentation: Filtering

- Best parameters for bilateral filter
Spatial: 30
Range: 110

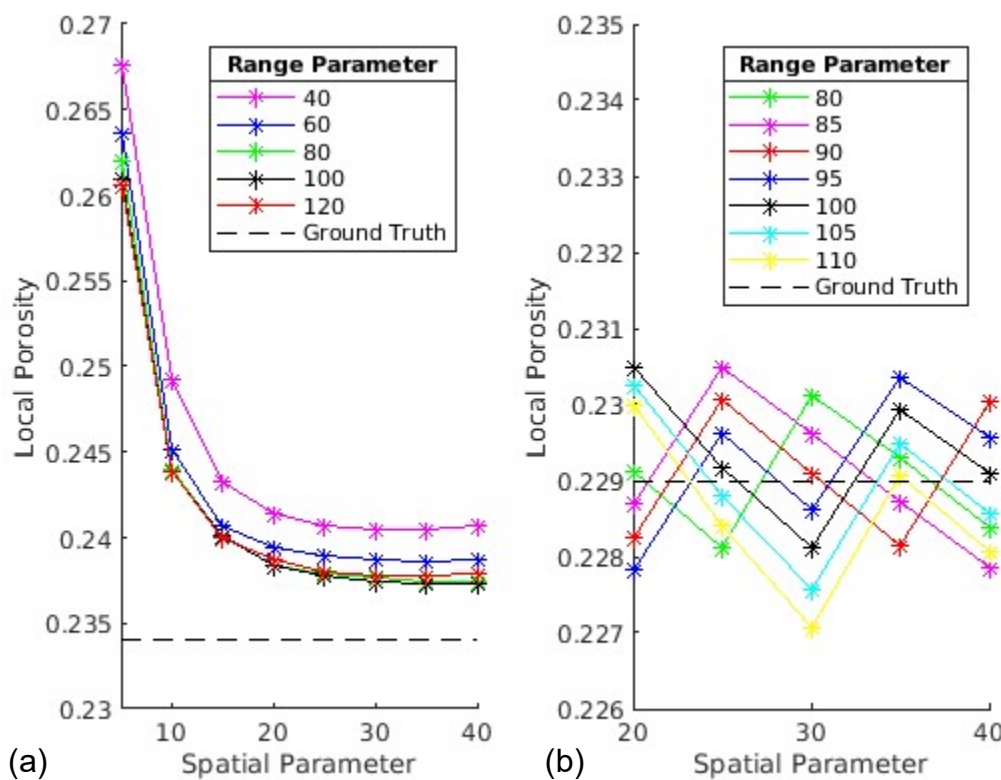


Fig. 14. Bilateral filter parameter sensitivity study on image (a) 1333 and (b) 200.

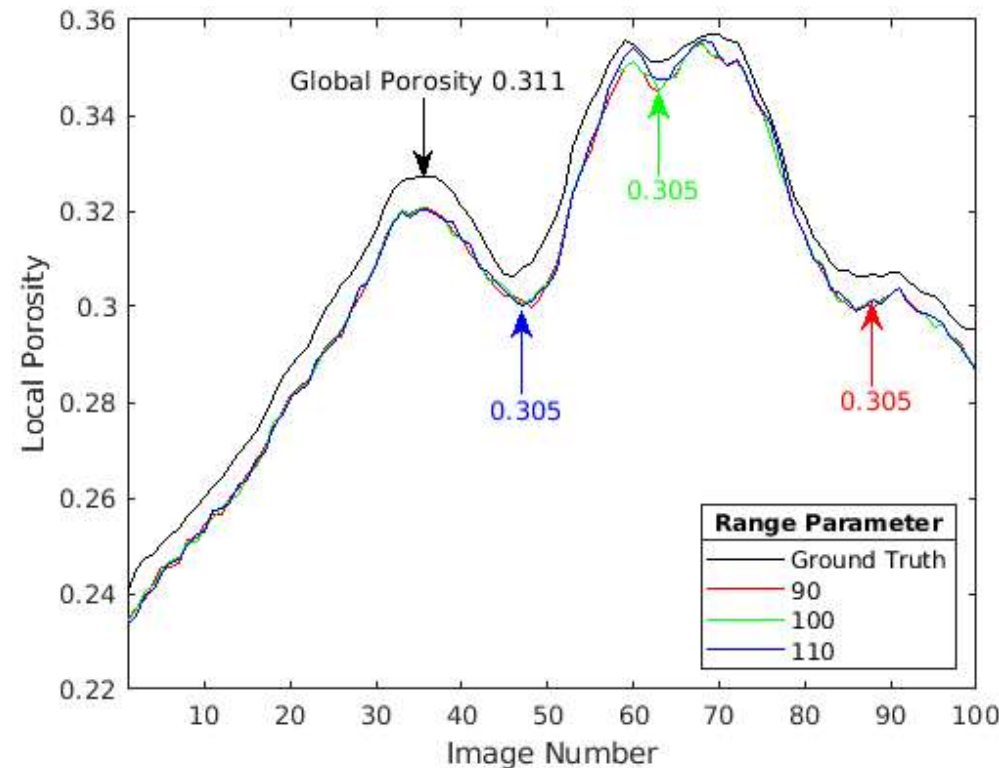


Fig. 15. Local and Global Porosity of $400 \times 400 \mu\text{m}^2$ image stack using selected parameter.

Image Segmentation

- For thresholding, Otsu's and Li's method performed the best.

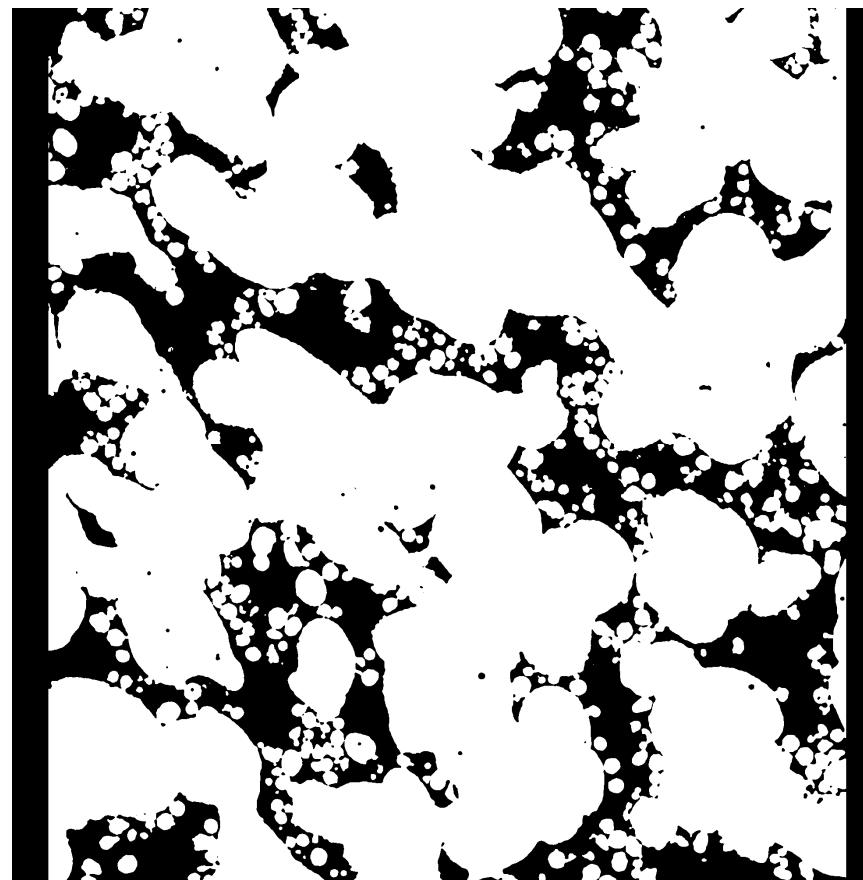


Fig. 12. Thresholded image 1308 1333 using Otsu's Method.

Image Segmentation: Thresholding

- For thresholding, Otsu's and Li's method performed the best.

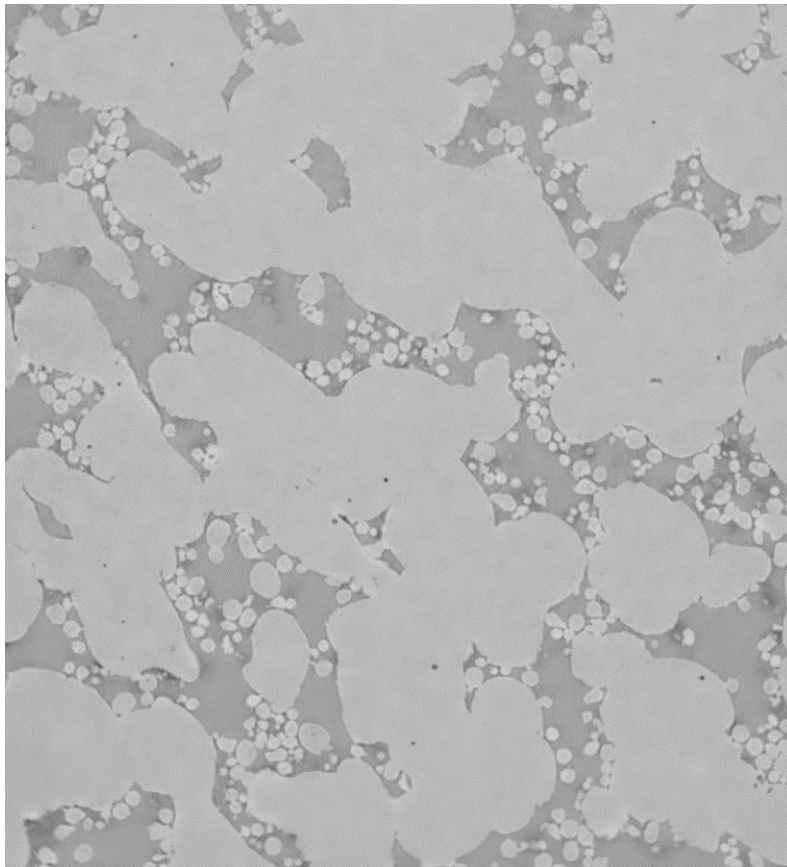


Fig. 11. Filtered image 1333

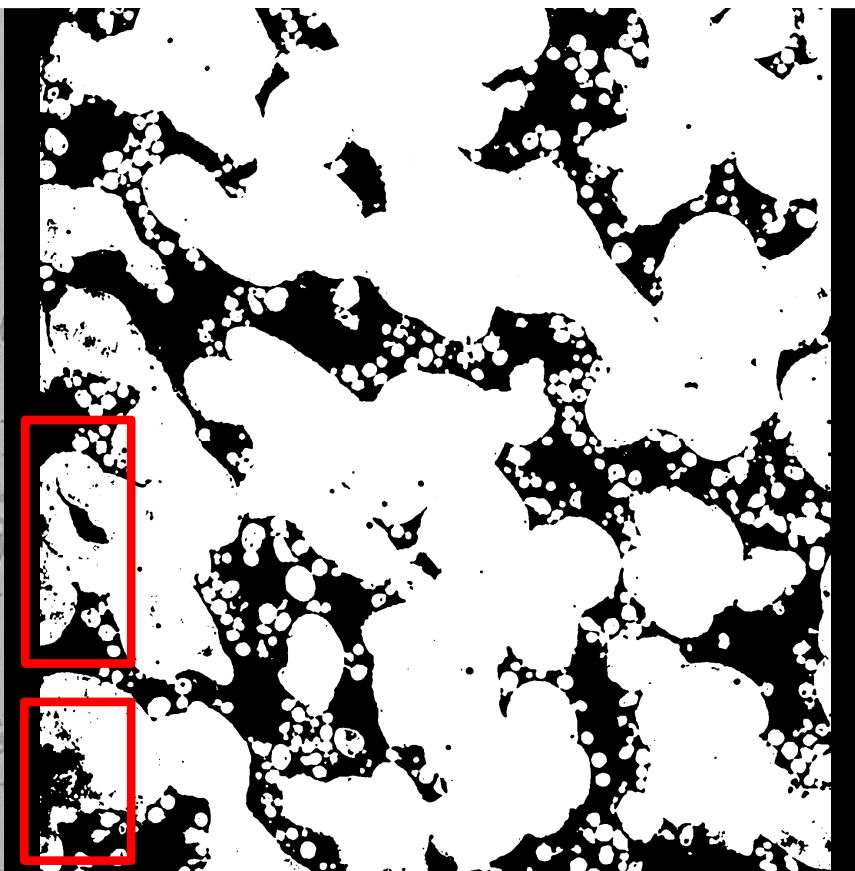


Fig. 16. Thresholded Image 1333 using mean method.

Image Segmentation: Thresholding

- For thresholding, Otsu's and Li's method performed the best.

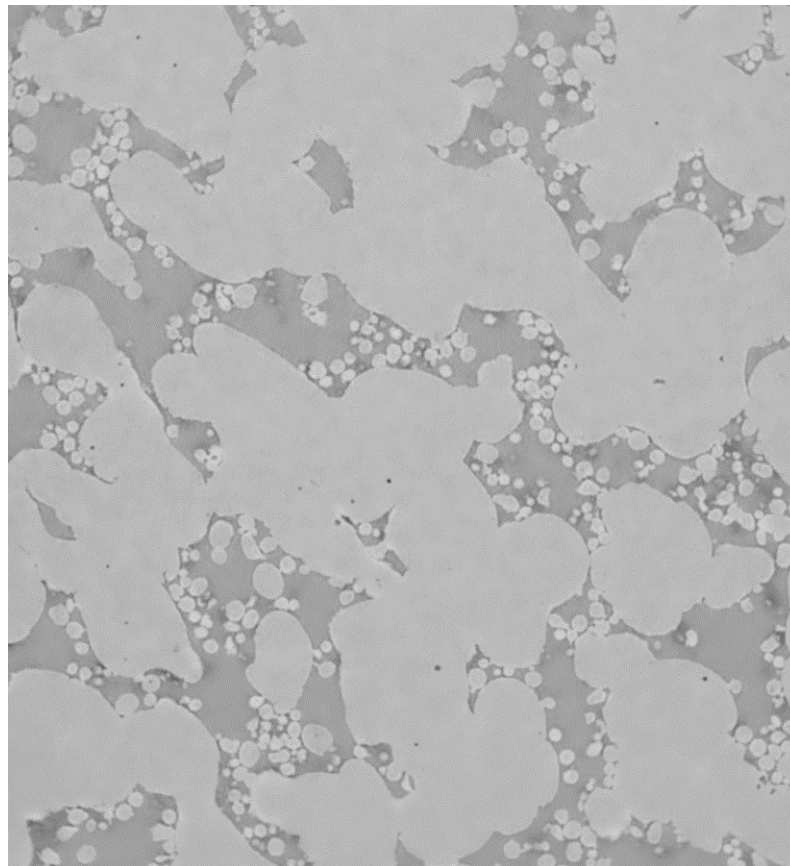


Fig. 11. Filtered image 1333

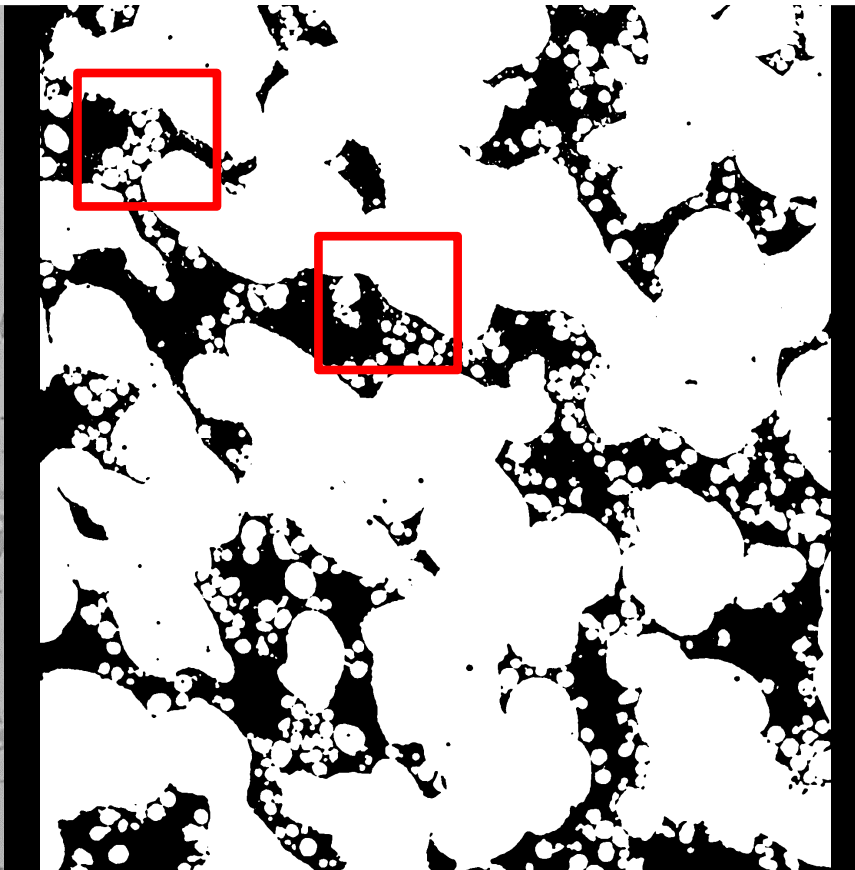


Fig. 17. Thresholded Image 1333 using moment method.

Image Segmentation: Thresholding

- For thresholding, Otsu's and Li's method performed the best.

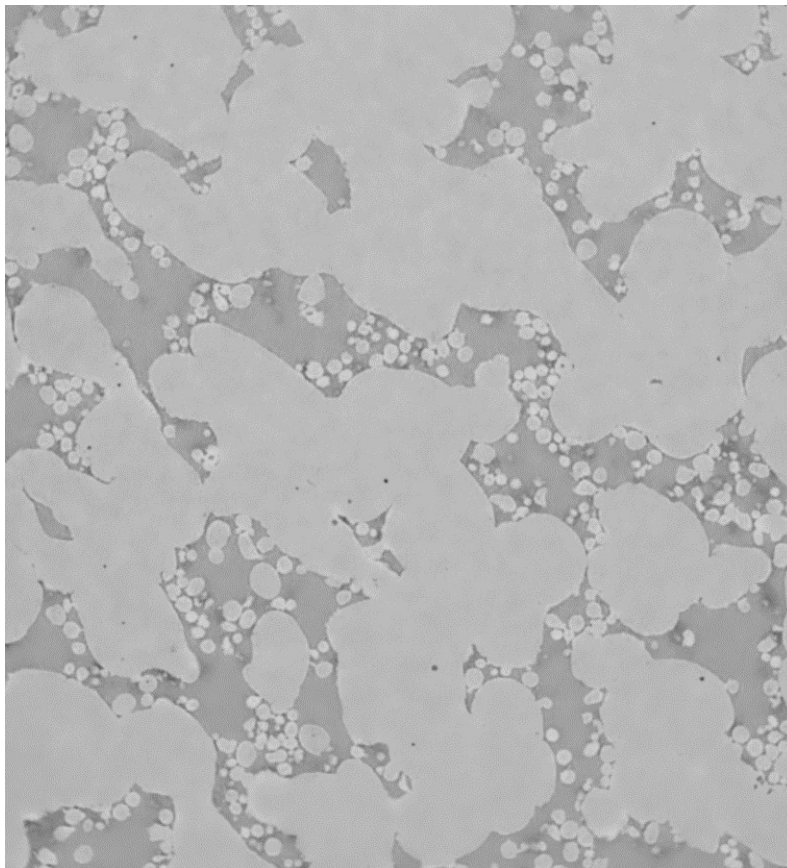


Fig. 11. Filtered image 1333

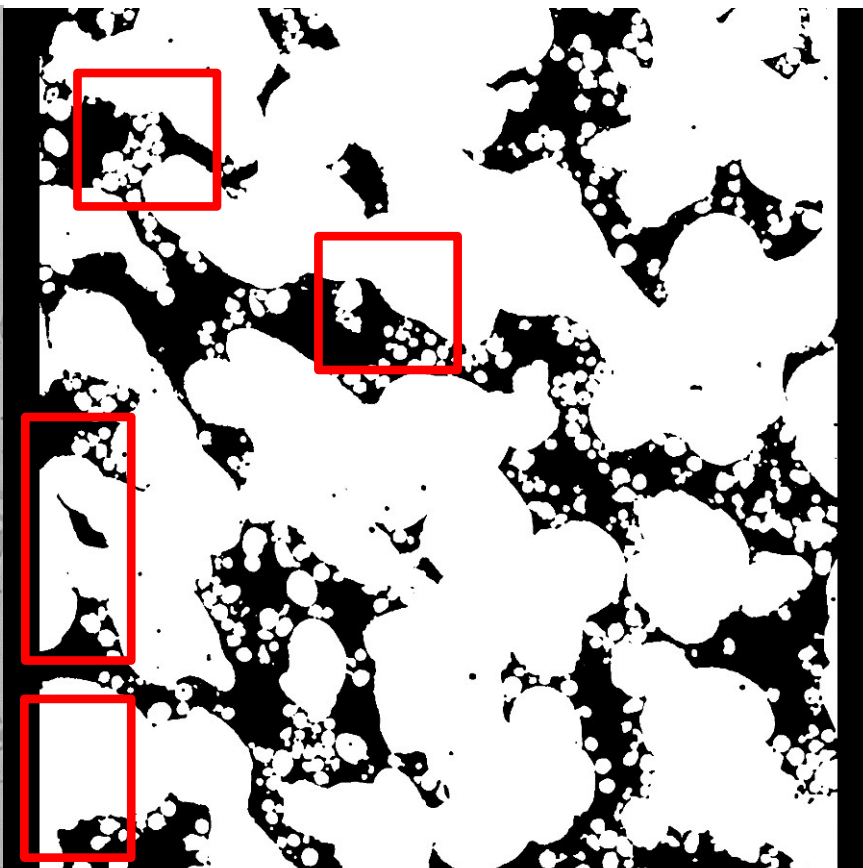


Fig. 12. Thresholded Image 1333 using Otsu's method.

Overview of Workflow

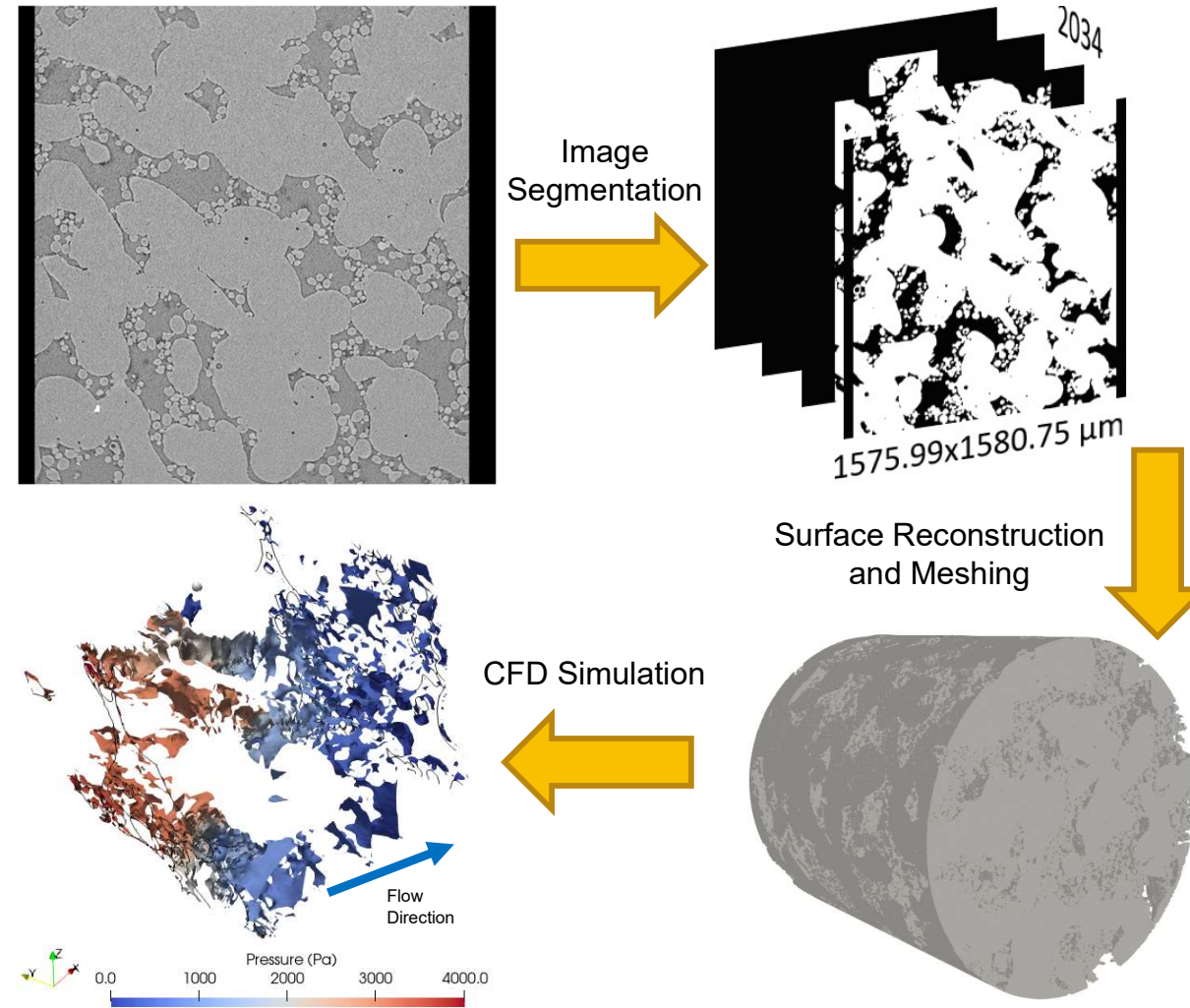


Fig. 8. Diagram of μ CT to CFD workflow.

Surface Reconstruction

- STL is generated in ParaView, however file size can be massive.
- A decimating algorithm reduces file size up to 70% without affecting porosity or predicted permeability.

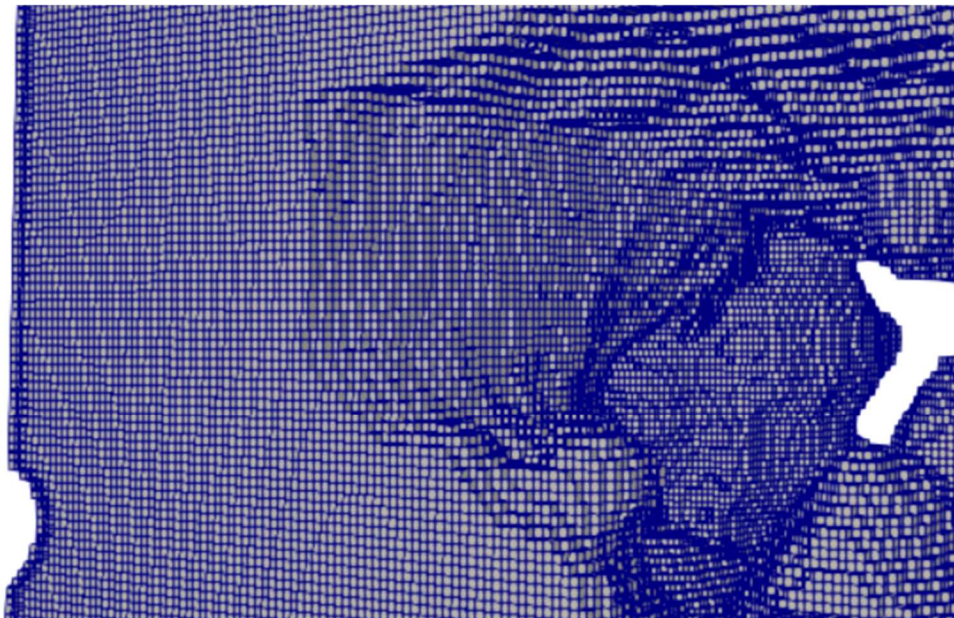


Fig. 18. Section of image stack showing solid volume



Fig. 19. Example of decimation

Surface Reconstruction

- STL is generated in ParaView, however file size can be massive.
- A decimating algorithm reduces file size up to 70% without affecting porosity or predicted permeability.

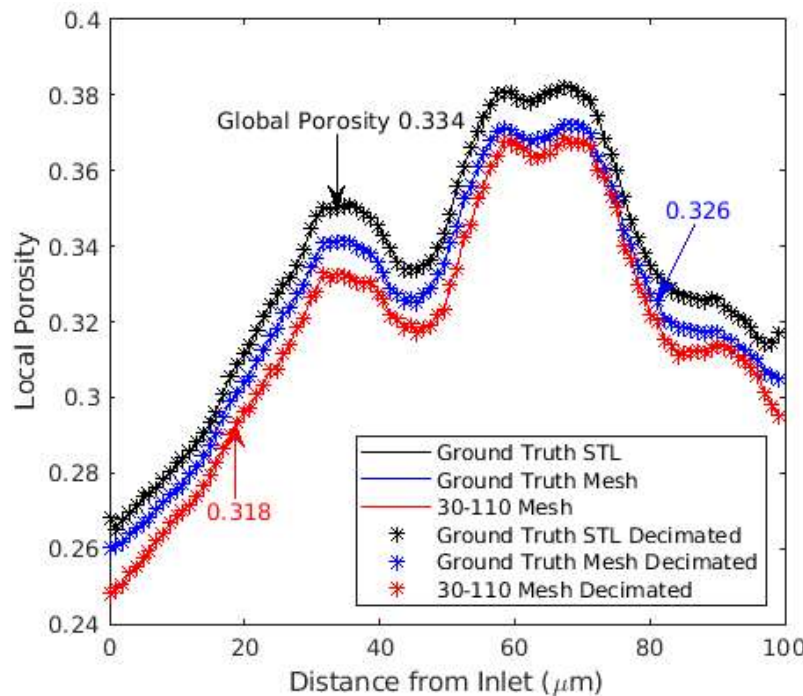


Fig. 20. Local and global porosity of ground truth STL, mesh of ground truth STL, mesh of auto-segmented 30-110 STL and effects of decimation.

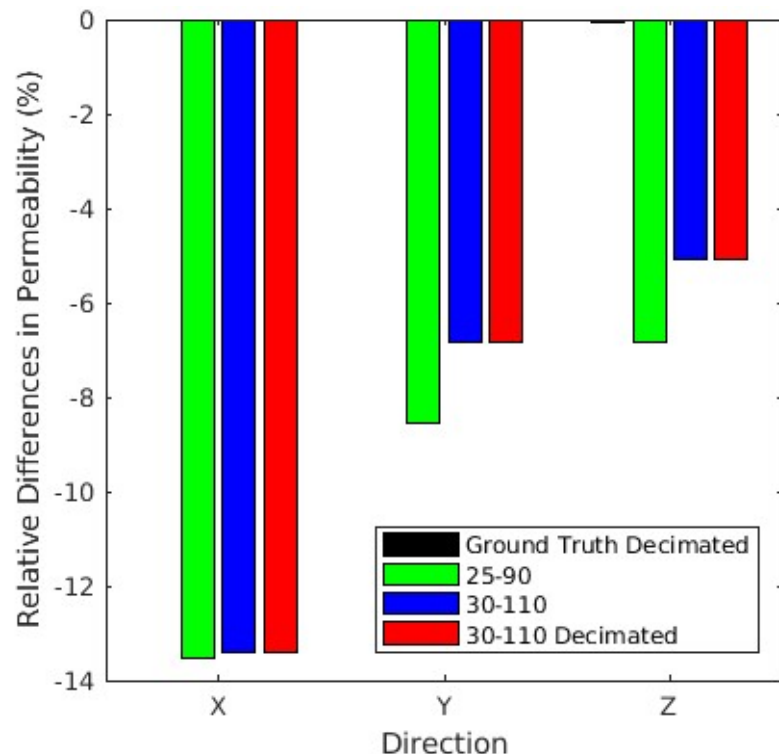


Fig. 21. Relative differences in anisotropic permeability of various meshes relative to ground truth simulation. (XX-YY refers to spatial and range parameter respectively)

Mesh Generation

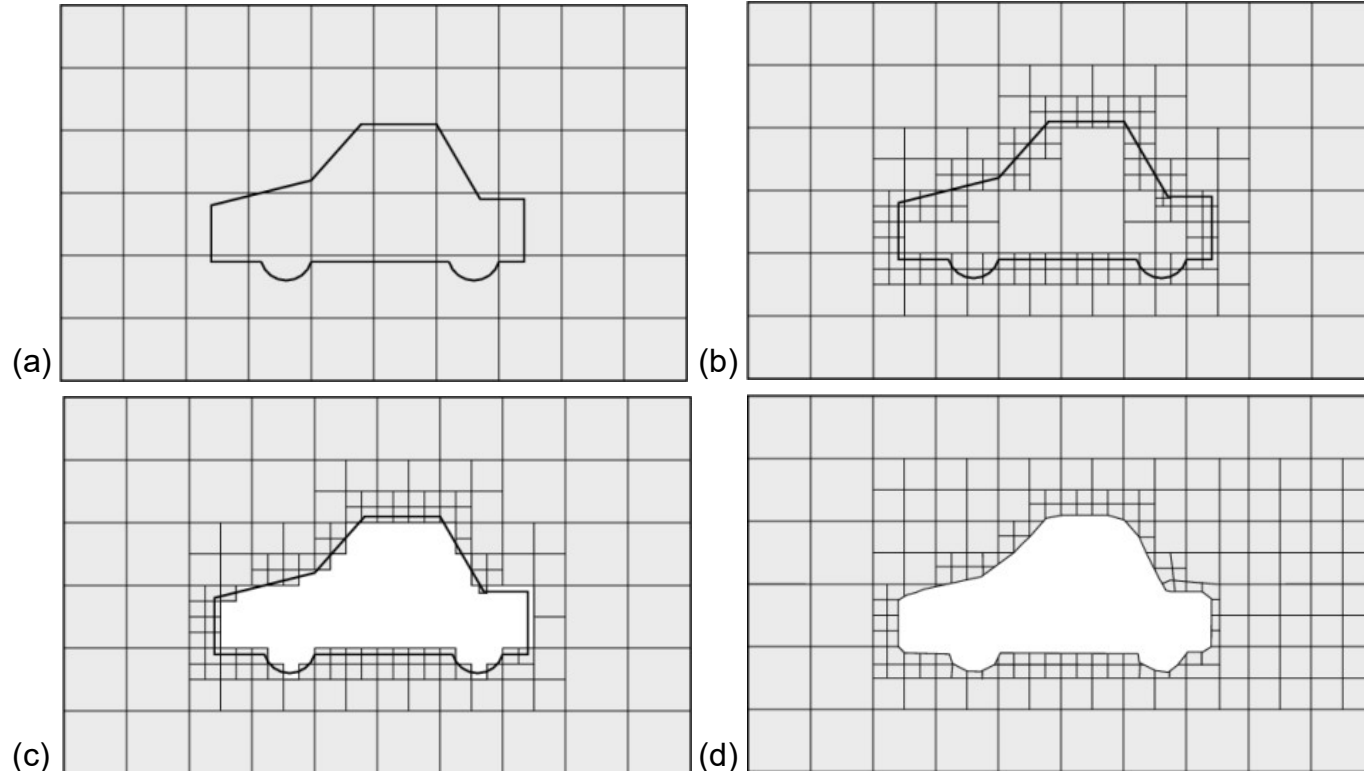


Fig. 22. *snappyHexMesh* meshing process (a) initial mesh with STL (b) cell splitting by surface (c) cell removal (d) surface snapping [6]

Mesh Generation

- A cropped 400 μm -cube volume is now analyzed using CFD.

Table 1. Mesh information and mesh quality using 30-110 decimated STL.

Number of Cells	
Polyhedra Cells	74,891
Hexahedra Cells	2,527,403
Total Cells	2,602,294
Mesh Quality Metrics	
Max Aspect Ratio	4
Non-Orthogonality	Avg/Max 8/48
Max Skewness	3

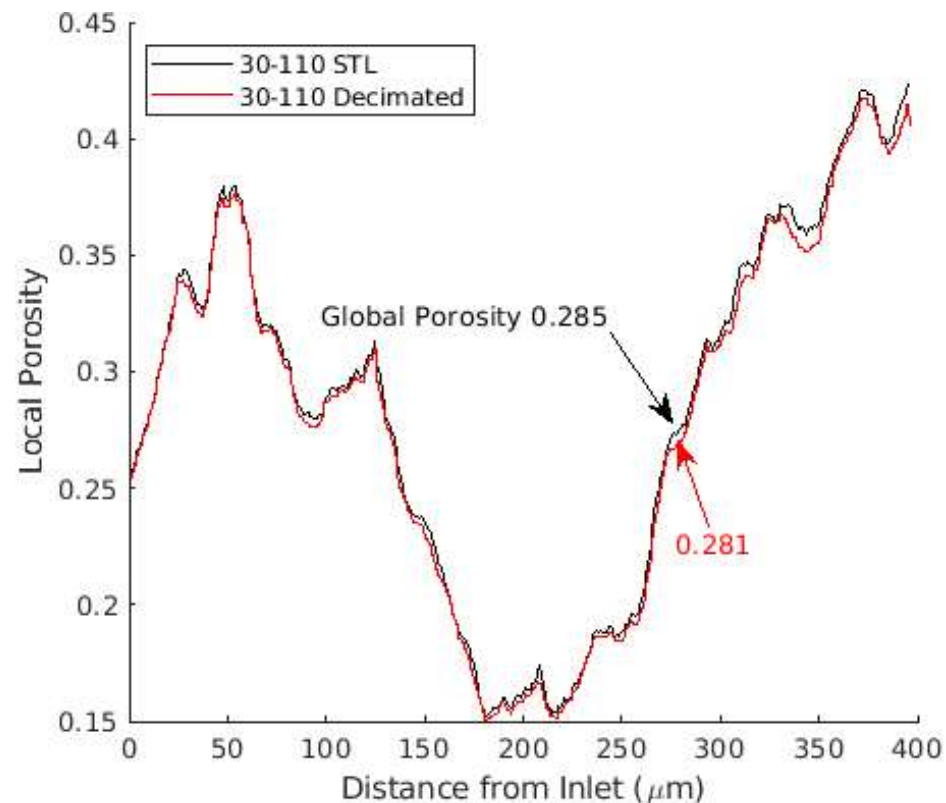


Fig. 23. Local and Global Porosity of 400x400x400 μm^3 volume STL and decimated mesh.

Case Setup

- Steady-state laminar simulations computed in OpenFOAM
- Simulated in x, y and z directions

Table 2. Fluid properties

Average Pore Diameter (μm)	70
Density (kg/m^3)	850
Viscosity ($\text{Pa}\cdot\text{s}$)	0.5
Reynolds Number	0.0001

Table 3. Velocity and pressure boundary conditions

Patch Name	Velocity (mm/s)	Pressure (m^2/s^2)
Inlet	fixedValue (0.1 0 0)	zeroGradient
Outlet	zeroGradient	fixedValue (0)
Walls	fixedValue (0 0 0)	zeroGradient
Wick	fixedValue (0 0 0)	zeroGradient

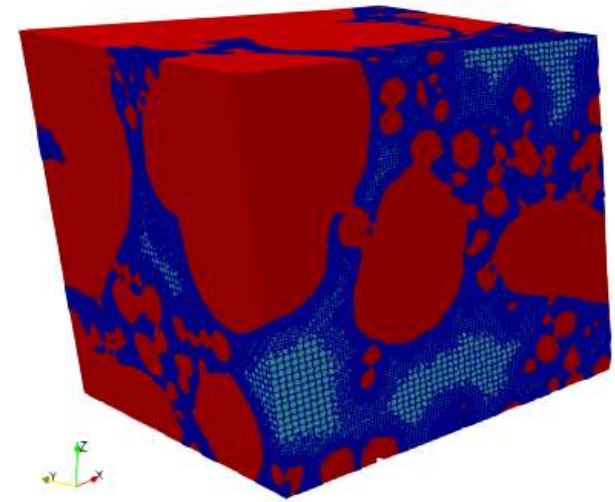


Fig. 7. $400 \times 400 \times 400 \mu\text{m}^3$ mesh for the fluid (blue) and solid (red) regions.

Results

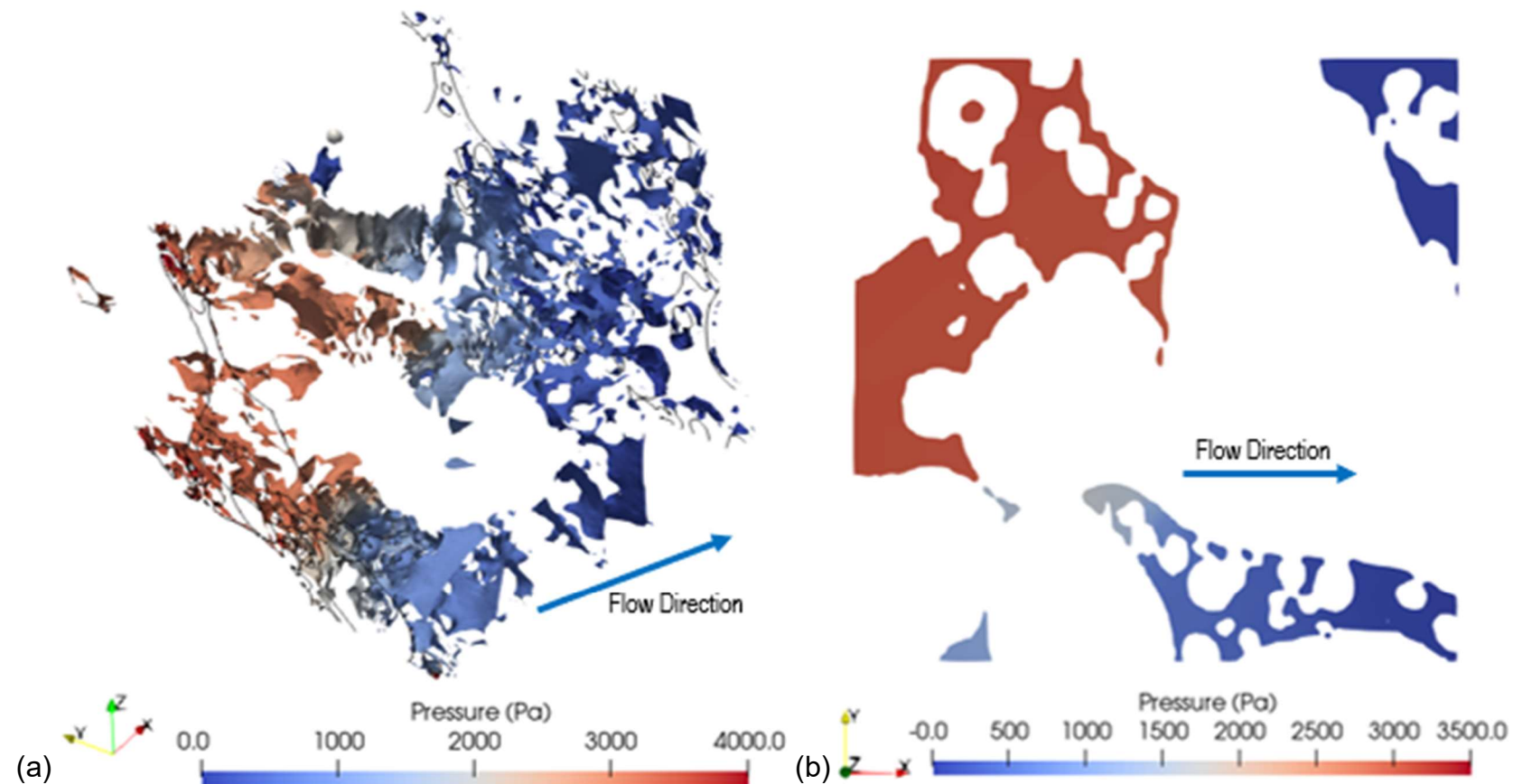


Fig. 24. Model simulation of (a) pressure contour (b) pressure distribution at $z = 1/2$ plane along flow direction

Results

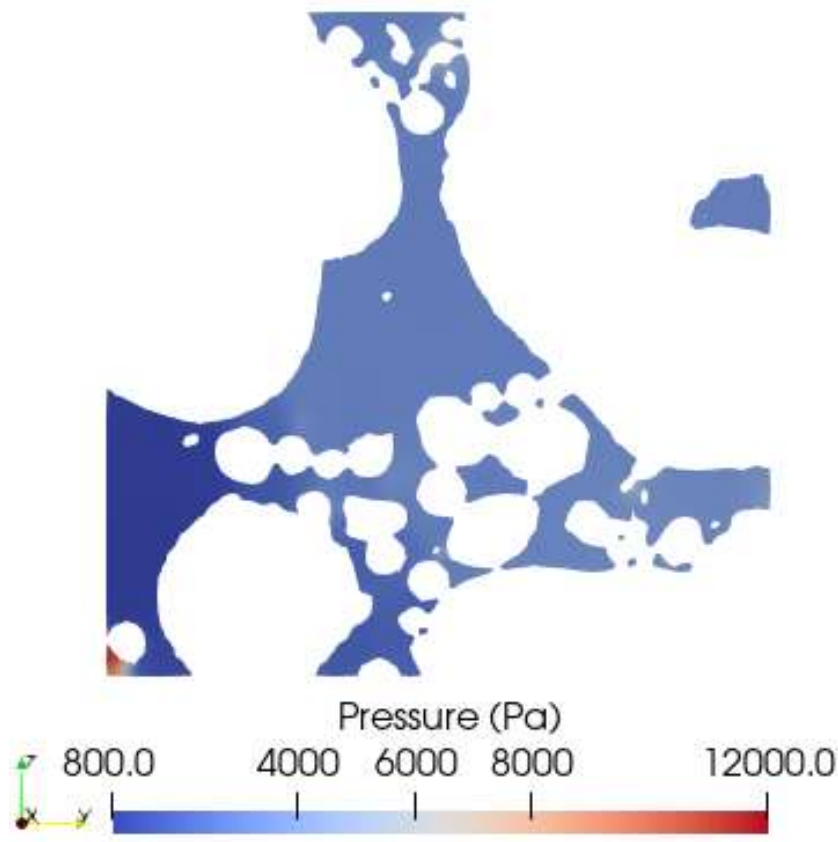


Fig. 25. Pressure distribution at the inlet.

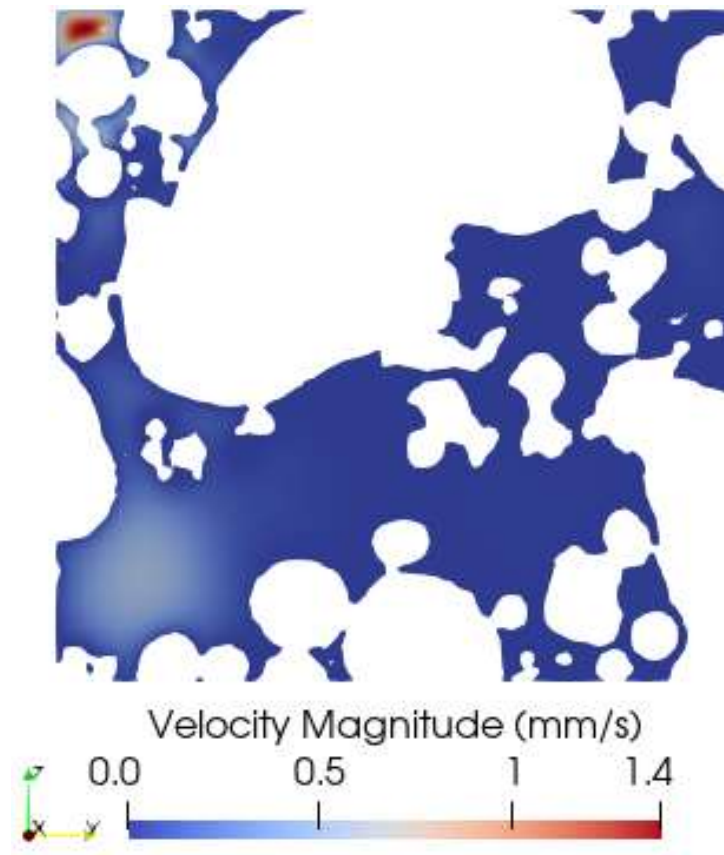


Fig. 26. Velocity distribution at the outlet.

Validation

- Using Darcy Law, we can calculate permeability

$$\kappa = \mu \langle u \rangle \frac{L}{\Delta P} \quad (1)$$

Table 4. Average velocity at outlet, pressure drop along wick and permeability estimate in x, y and z directions

Direction	Average Velocity (mm/s)	Pressure Drop (Pa)	κ (m ²)
x	0.025	2704	1.81E-12
y	0.051	6008	1.66E-12
z	0.036	4369	1.63E-12

- We can validate the solution using Carman-Kozeny equation

$$\kappa = \Phi_s^2 \frac{\varepsilon^2 D^2}{180(1-\varepsilon)^2} \quad (2)$$

- Applying some assumption, we obtain $\kappa = 1.23e-12$ m²

Scalability

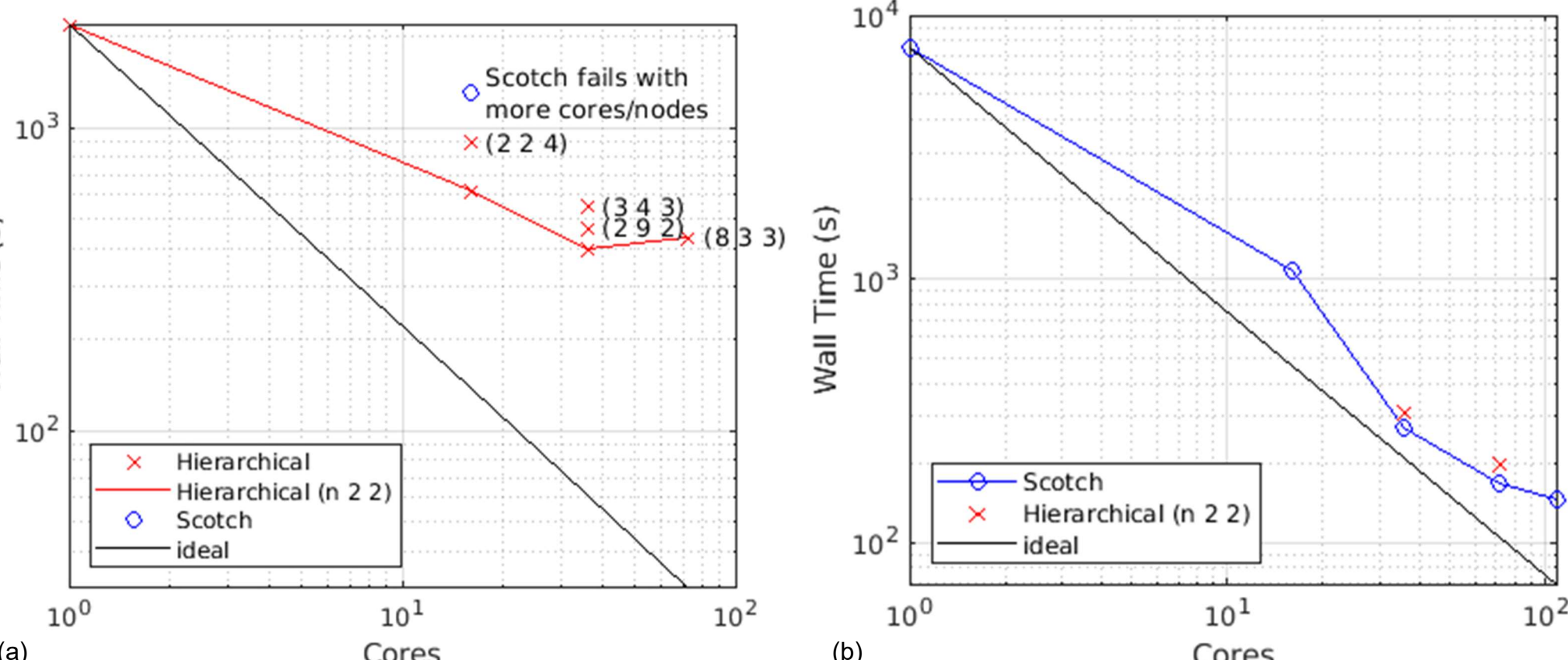


Fig. 27. Scaling of scotch and hierarchical domain decomposition method using BeoShock for (a) snappyHexMesh (b) simpleFoam

Conclusion and Future Work

- Bilateral filtering and Otsu's thresholding can enable automatic image segmentation from μ CT data.
- Pore surface can be reconstructed to generate detailed and high-quality mesh.
- CFD can accurately predict permeability and provide detailed view of velocity and pressure distribution along the wick.
- Future work will investigate effect of a larger sample

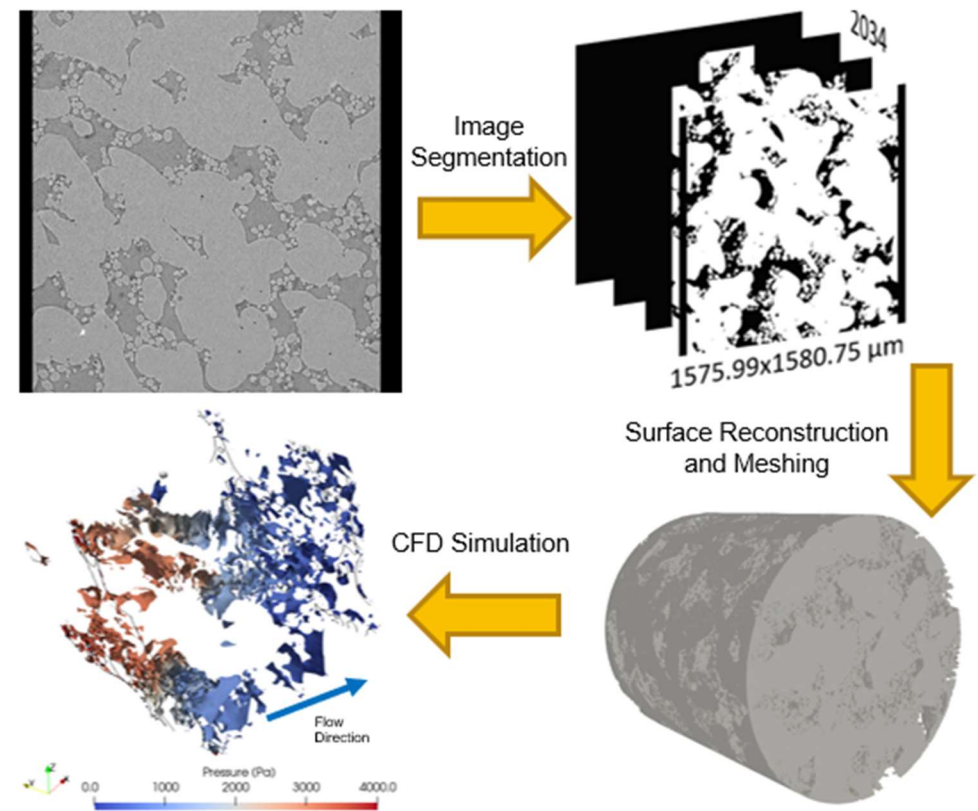


Fig. 8. Diagram of μ CT to CFD workflow.



Questions?

Meshering and Pore-Scale Simulation of Additively Manufactured Wicks in OpenFOAM

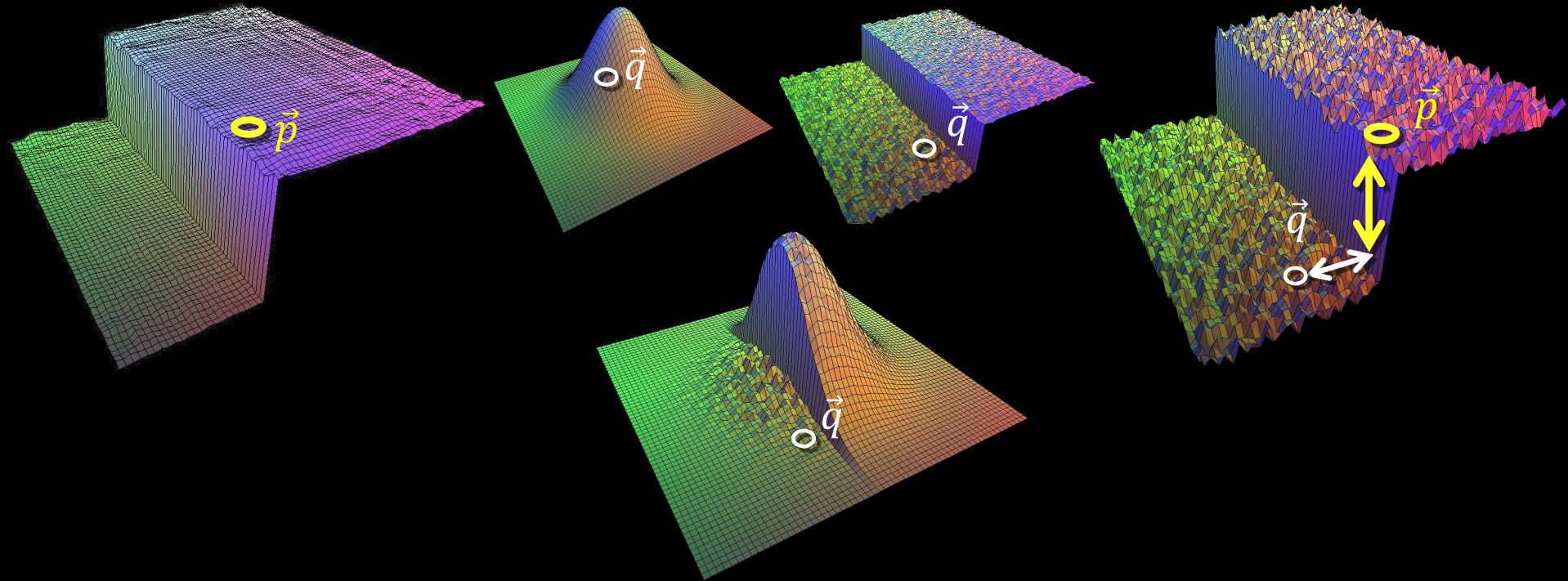
Marcus Ang

Department of Mechanical Engineering
Wichita State University

4/7/2023

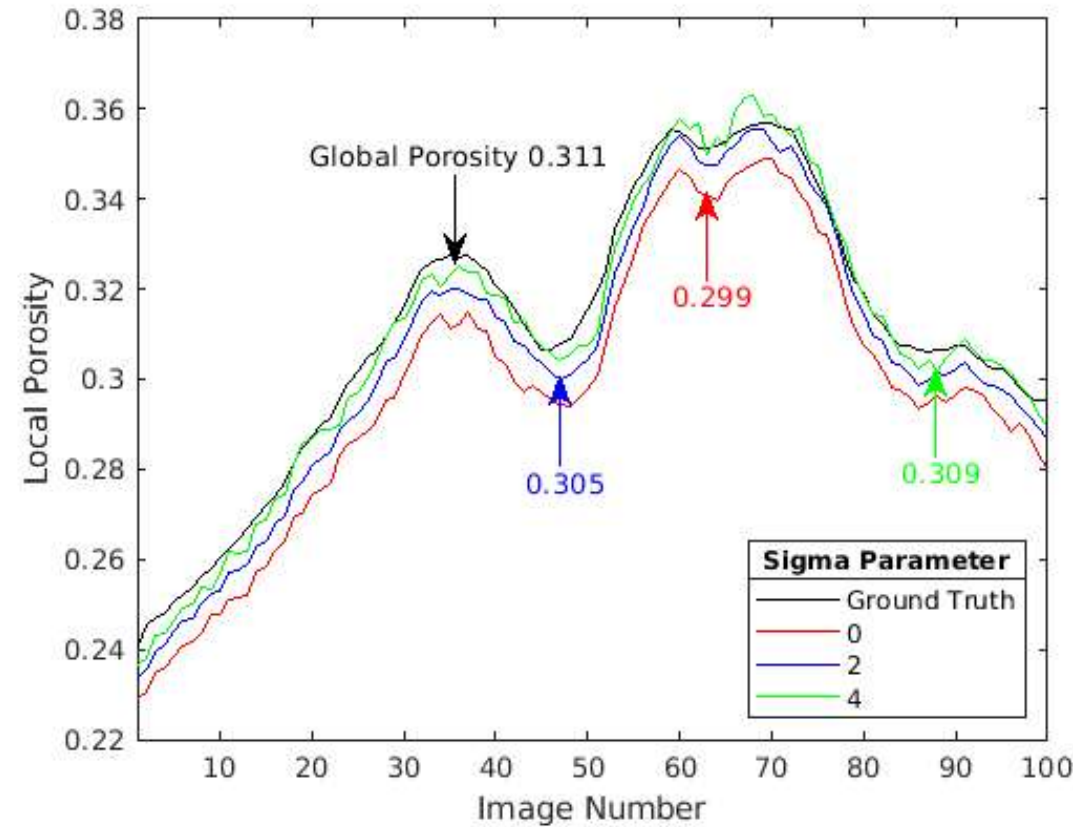
Supplemental Material: Bilateral Filter

$$BF[I]_{\mathbf{p}} = \frac{1}{W_p} \sum_{\mathbf{q} \in S} G_{\sigma_s}(\|\mathbf{p} - \mathbf{q}\|) G_{\sigma_r}(|I_p - I_q|) I_q \quad (1)$$



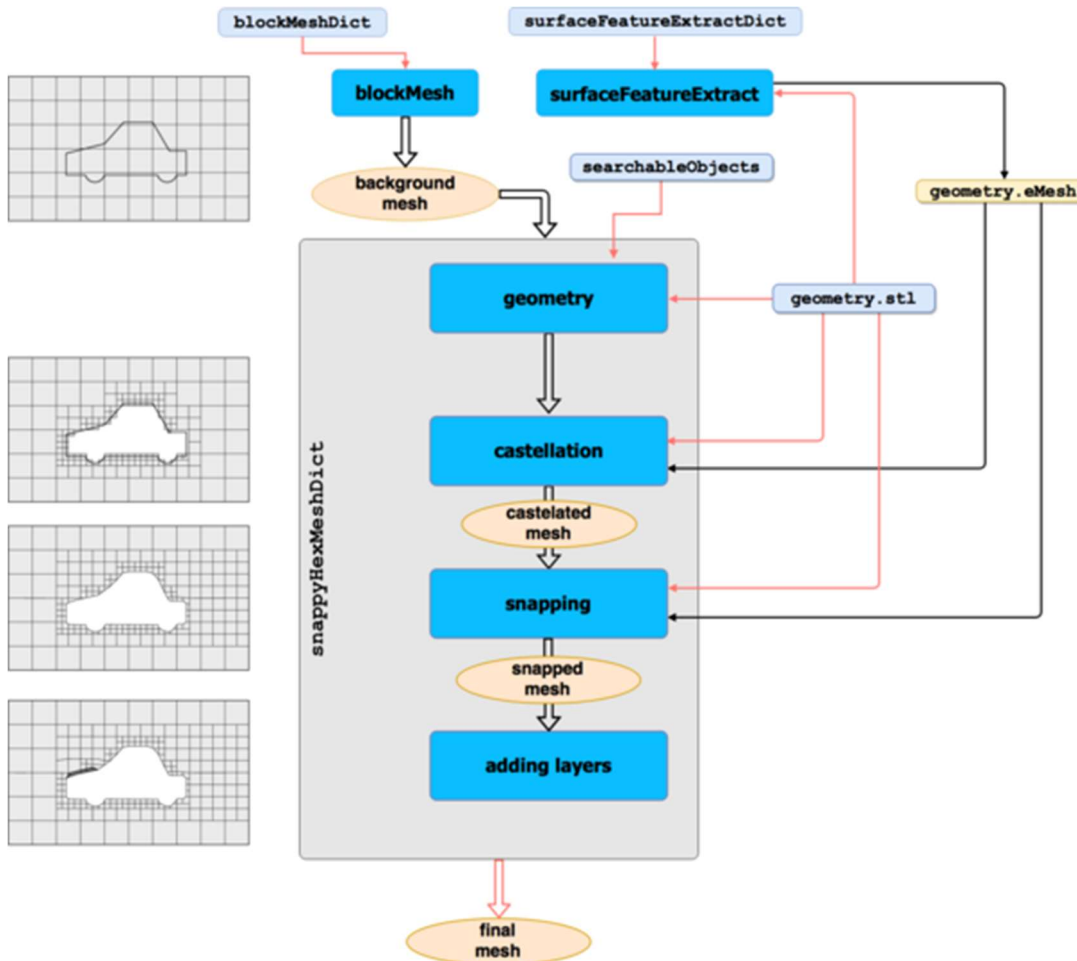
$$W_{\vec{p}} = \sum_{\mathbf{q} \in S} G_{\sigma_s}(\|\mathbf{p} - \mathbf{q}\|) G_{\sigma_r}(|I_p - I_q|) \quad (2)$$

Supplemental Material: Additional Gaussian Blur



Supplemental Material: snappyHexMesh

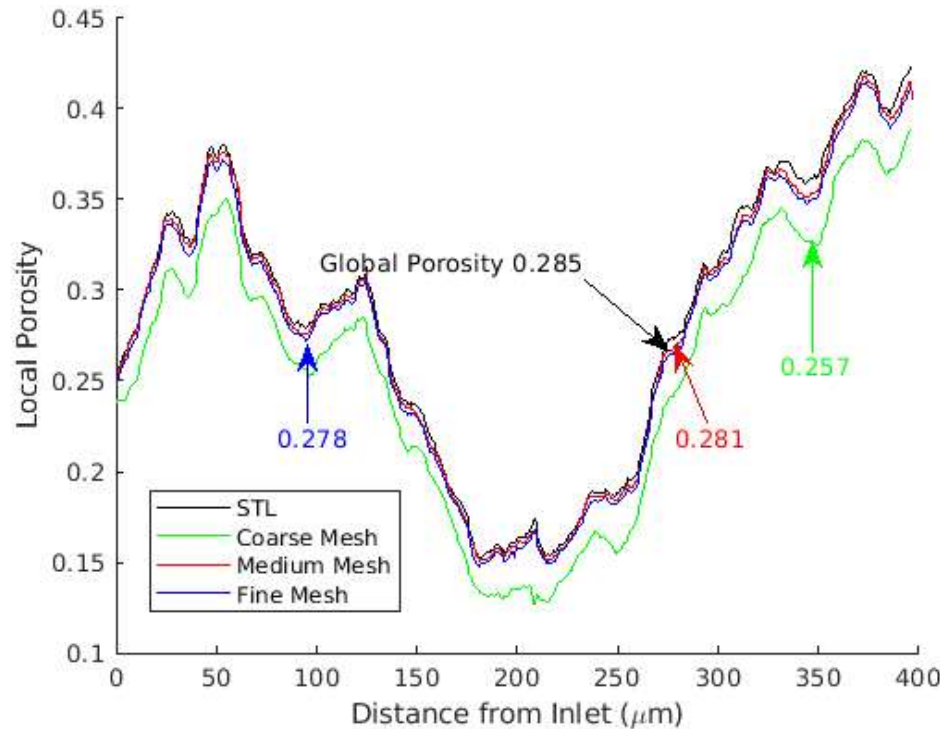
- OpenFOAM's native mesh generator



```
castellatedMeshControls
{
    minRefinementCells 10;
    nCellsBetweenLevels 4;
    features
    (
        { 'Wick.eMesh';
          level 4; }
    );
    refinementSurfaces
    { Wick
      { level (4 4); }
    }
    ...
}

snapControls
{
    nSmoothPatch 4;
    tolerance 0.1;
    nSolvIter 2;
    nRelaxIter 1;
    nFeatureSnapIter 1;
    ...
}
```

Supplemental Material: Grid Independence Study



Mesh	Number of Cells	Porosity	$\kappa (\text{m}^2)$	Area of Inlet (m^2)	Pressure Drop (Pa)	Average Velocity at Outlet(m/s)
Coarse	401,973	0.257	1.816E-12	3.738E-08	2.702E+03	2.476E-05
Medium	2,602,294	0.281	1.815E-12	3.884E-08	3.972E-02	2.476E-05
Fine	13,991,853	0.278	1.606E-12	3.940E-08	3.055E+03	2.476E-05

Supplemental Material: Numerical Schemes

- Steady-state solver for incompressible laminar or turbulent flow using the SIMPLE (Semi-Implicit Method for Pressure Linked Equations) algorithm to solve the Navier-Stokes equations.

$$\nabla \cdot \vec{u} = 0 \quad (1)$$

$$\vec{u} \cdot (\nabla \cdot \vec{u}) - \nabla \cdot (v \nabla \vec{u}) = -\nabla p \quad (2)$$

- gradSchemes: cellIMDLimited Gauss linear 0.5;
divSchemes: Gauss linearUpwind grad(U);
laplacianSchemes: Gauss linear limited 0.777;
- P: GAMG solver with GaussSeidel smoother
U: PBiCGStab solver with DILU pre-conditioner
nCorrectors: 3
nNonOrthogonalCorrectors: 1
relaxationFactors: U - 0.7, P - 0.3